applied sciences

MDPI

Communication

Prediction of Carlson Trophic State Index of Small Inland Water from UAV-Based Multispectral Image Modeling

Cheng-Yun Lin [1,2,3], Ming-Shiun Tsai [4], Jeff T. H. Tsai [5] and Chih-Cheng Lu [1,2,4,*]

[1] Department of Mechanical Engineering, National Taipei University of Technology, Taipei 106, Taiwan
[2] College of Mechanical and Electrical Engineering, National Taipei University of Technology, Taipei 106, Taiwan
[3] Rdata System Co., Ltd., Taichung 406, Taiwan
[4] Graduate Institute of Mechatronic Engineering, National Taipei University of Technology, Taipei 106, Taiwan
[5] Department of Optoelectronics and Material Sciences, National Taiwan Ocean University, Keelung 202, Taiwan
* Correspondence: cclu23@mail.ntut.edu.tw; Tel.: +886-2-2771-2171 (ext. 2067)

Abstract: This paper demonstrates a predictive method for the spatially explicit and periodic in situ monitoring of surface water quality in a small lake using an unmanned aerial vehicle (UAV), equipped with a multi-spectrometer. According to the reflectance of different substances in different spectral bands, multiple regression analyses are used to determine the models that comprise the most relevant band combinations from the multispectral images for the eutrophication assessment of lake water. The relevant eutrophication parameters, such as chlorophyll a, total phosphorus, transparency and dissolved oxygen, are, thus, evaluated and expressed by these regression models. Our experiments find that the predicted eutrophication parameters from the corresponding regression models may generally exhibit good linear results with the coefficients of determination (R^2) ranging from 0.7339 to 0.9406. In addition, the result of Carlson trophic state index (CTSI), determined by the on-site water quality sampling data, is found to be rather consistent with the predicted results using the regression model data proposed in this research. The maximal error in CTSI accuracy is as low as 1.4% and the root mean square error (RMSE) is only 0.6624, which reveals the great potential of low-altitude drones equipped with multispectrometers in real-time monitoring and evaluation of the trophic status of a surface water body in an ecosystem.

Keywords: multispectral image; unmanned aerial vehicle (UAV); Carlson trophic state index (CTSI); water quality; ecosystem

Citation: Lin, C.-Y.; Tsai, M.-S.; Tsai, J.T.H.; Lu, C.-C. Prediction of Carlson Trophic State Index of Small Inland Water from UAV-Based Multispectral Image Modeling. *Appl. Sci.* **2023**, *13*, 451. https://doi.org/10.3390/app13010451

Academic Editor: Yosoon Choi

Received: 8 November 2022
Revised: 12 December 2022
Accepted: 21 December 2022
Published: 29 December 2022

1. Introduction

Clean water is an indispensable element for people's livelihood, industries and agriculture; thus, water resources are considered one of the most important assets for live creatures worldwide. Hence, it is necessary to manage and monitor water quality all the time. Many developing countries in the world where the ensuing industrialization and urbanization driven by rapid economic development have brought about tremendous pressure to the environment [1–5]. In many cities, pollution can be easily and rapidly spread from industrial areas to nearby residential areas and even reservoir catchment areas because the vicinity is very small. Although Taiwan is an area rich in water resources, its land area is so small that water storage is not as easy as imagined. In addition, due to global warming in recent years, each country on earth has been affected to varying degrees by extreme climate. Facing the problem of instantaneous high-intensity rainstorms or prolonged droughts, the water quality in various catchment areas will be unstable; hence, real-time water quality management is extremely important [6–9]. Although the current commonly used water quality monitoring equipment has good reliability, some conventional monitors (e.g., pH meters, conductivity meters, etc.) must be manually calibrated

and regularly cleaned, while traditional water quality analysis methods rely on on-site sampling and measurement and chemical analysis in the laboratory. All these require a lot of manpower, many material and financial resources and huge time cost. Moreover, due to the limited monitoring points, they cannot reflect immediate temporal and spatial changes in water quality. Based on the abovementioned fact, the macro real-time monitoring of water quality changes must be conducted, such that relevant departments can grasp the water environment and dynamically track and analyze water pollution and other events in time.

Remote sensing technology, which can measure and monitor the water environment transition macroscopically and in real time, is introduced into the field of water quality monitoring to overcome the abovementioned shortcomings of traditional methods and meet the needs of water quality monitoring. Since NASA's launch of three satellites (i.e., Nimbus-7, TIROS-N and Seasat) related to ocean observation in 1978, more and more sensors have been used for water quality monitoring. The main data sources of water quality monitoring can be divided into multispectral imaging data, hyperspectral imaging data and non-imaging spectral data. Multispectral image data, such as Landsat Thematic Mapper (TM) images, are relatively easy to obtain; hence, they have been widely used in the quantitative remote sensing of water quality around the world. In addition, based on an in-depth understanding of the mechanism and principles of radiation propagation in water, many scholars have begun to devote time to improving the existing water quality remote sensing monitoring algorithms to further improve the inversion accuracy. López-García and Caselles were the first researchers to study the trophic status of Albufera in Valencia Lake (Valencia, Spain) using Landsat-TM data [10]. They obtained empirical models of chlorophyll a and seston particles using TM band 1 (452–518 nm), but were unable to define a transparency model. Domínguez et al. studied the nutritional status of lakes/ponds in the Southeast Regional Park, 20 km southeast of Madrid, Spain, and proposed a chlorophyll a and transparency model using TM band 2 (528–609 nm) and for the concentration of the total suspended particles using TM band 4 (776–904 nm) [11]. Further, with the continuous deepening of research on the spectral characteristics of the water quality parameters and the advancement of algorithmic research methods, water quality monitoring technology via remote sensing has been developed, from qualitative to quantitative modes. In addition to the parameters of chlorophyll a, suspended solids and yellow substances, the water quality parameters also include turbidity, chemical oxygen demand, five-day biochemical oxygen demand (BOD5), transparency, total phosphorus and total nitrogen, etc. [12–20].

Multispectral imaging uses different objects to acquire different reflection characteristics for each band spectrum, which is very convenient for resource investigation and environmental exploration. Traditionally, the carriers used to collect multispectral images using satellites and aviation aircraft or ground surveys. At present, some research groups still use satellite telemetry technology to obtain spectral image information for analysis. However, the use of satellite remote sensing influencing systems or the regular monitoring of aquatic ecosystems has two main limitations: First, the significant disturbance to the atmosphere, which may prevent observers from immediately obtaining information for a long time. Second, the poorer spatial resolution of the remote sensing on the satellite. In general, multispectral sensors designed for water applications are mainly used for seawater monitoring (e.g., medium-resolution imaging spectrometers, ocean and land color instrument), but their spatial resolution will be coarser and can detect larger areas. Therefore, the sensors currently used to monitor most inland waters are those originally designed for onshore applications, such as the Sentinel 2 Multispectrometer (MSI) and the Landsat 8 Operational Land Imager. These facts will lead to limitations of the regression model and an inversion of the accuracy. In addition, the multispectral image data collected by traditional satellites and aircraft face the problems of a long cycle time, high cost and the meter-level resolution. Fortunately, with the development of modern telemetry technology and improvements in computing power and camera image resolution, the data obtained in recent years are more accurate and realistic. More importantly, as the emerging development of

unmanned aerial vehicle (UAV) technology becomes more mature, image resolution has been reduced from meters to centimeters. Drones are being widely employed in the logistic, commercial, precision agriculture, military defense and national security fields. Recently, a vast amount of research literature, particularly in the multispectral imaging as well as remote sensing results (with satellite or UAV), has been published for the application fields of water quality monitoring or prediction [21–25], bathymetry modeling [26], atmospheric observation [27], vegetation index evaluation [28–31] and precision agriculture [32–34], etc. Using a drone equipped with a multispectrometric instrument to collect multispectral image data during low-altitude flight can make the image resolution reach a level higher than the standard, consequently greatly improving the details of the multispectral image and the ability to interpret the characteristics of ground objects or water bodies.

Based on these facts and merits, a drone equipped with a multispectrometer was proposed to acquire image data. The optical raw data were then converted into reflectance for numerical regression analysis. On the other hand, the water samples simultaneously collected were sent to Taiwan SGS Co., Ltd. for biochemical analysis and validation of water quality parameters, which are introduced to the reflectance of five multispectral bands as to obtain the optimal regression models in terms of multispectral band combination for water quality parameters. To explore more possibilities of interpretation models, algorithmic research includes linear, band ratio and even logarithmic regression for multi-band expression. With these water parametric models, Carlson trophic state index (CTSI), representing the benchmark of water pollution status, can be acquired and predicted for the first time through optical image data and sampling analysis results, respectively. This proposed method is expected to more rapidly and economically monitor the water quality revolution of small-area surface water than traditional methods in a more efficient way.

2. The Experimental Site

As shown in Figure 1, Sun Moon Pond, located in Taichung Park, Taiwan, was selected as the research area for studying the influence of urbanization on the human living environment. Sun Moon Pond was originally a natural pond formed by a river passing by. Due to the population density increase, it was later artificially transformed into a leisure place for residents. The pond has a total area of approximately 14,000 m^2, with an average depth of 1.4 m and a total water storage capacity of approximately 19,600 m^3. The specific area is an artificial pond located in the center of the city, and only 20 tons of groundwater is introduced every day; thus, the bottom soil is heavily silted and algae bloom in water.

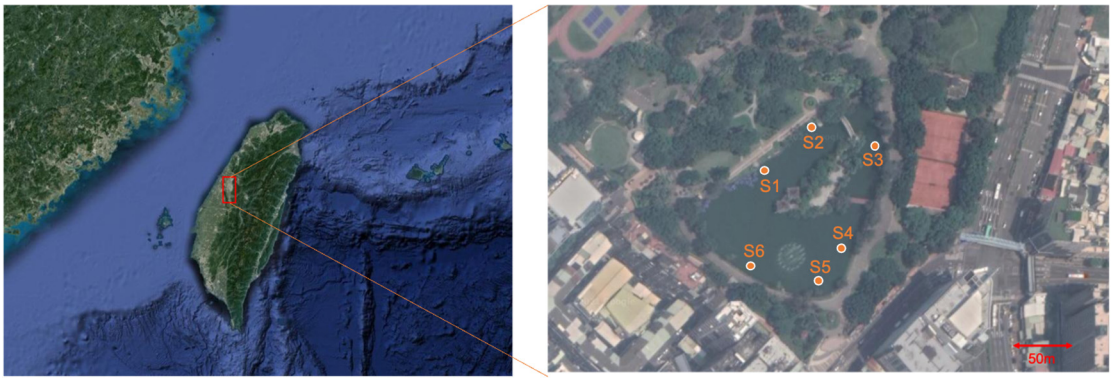

Figure 1. A map of Sun Moon Pond, Taichung city, Taiwan (available from Google Earth), where S1~S6 indicate the approximate positions of the sampling sites.

The pond has artificially stocked fish, turtles, ducks, geese, pigeons and other animals because it is a place for residents to relax and be entertained. The remaining feed and excrement of these animals can cause significant pollution, resulting in a peculiar smell and a high turbidity in the pond, which leads to severe eutrophication. In addition, this experimental site is located in the living environment of humans; therefore, the water (e.g.,

groundwater or irrigation water) pollution that this would potentially cause will be very dangerous to humans and other organisms. Considering the abovementioned reasons, Sun Moon Pond provides a good example of an ecosystem that requires preventive monitoring and regular control.

3. Methods

3.1. In Situ Data Collection

The water sampling data were taken at the same time as the multispectral images taken on site and further analyzed and verified by SGS (Société Générale de Surveillance) Ltd., Taiwan. Four water quality parameters (i.e., chlorophyll a concentration, total phosphorus, transparency and dissolved oxygen) were collected based on the water environment monitoring norms. The collected water samples were sent to SGS, Taiwan, for inspection. The test standards of water quality parameters in Taiwan are readily available [35]. For chlorophyll a inspection, the water sample was filtered using glass-fiber filter paper. The filter paper was then ground with a tissue grinder in 90% acetone solution to extract chlorophyll a. Subsequently, the extract absorbance was measured with a spectrophotometer to calculate the chlorophyll a concentration in the water sample. The detection method for the total phosphorus is as follows: the water sample was digested with sulfuric acid and persulfate to convert phosphorus into orthophosphate; ammonium molybdate and potassium antimony tartrate were added to react with orthophosphate to generate phosphomolybdic acid, which was reduced to blue by ascorbic acid; and finally, the color complex molybdenum blue was quantified by measuring its absorbance at 880 nm wavelength using a spectrophotometer. Transparency refers to the degree to which light can penetrate water. This method uses a Secchi disk or tube to measure the distance from the water surface to its visibility, which is the transparency of the water body, known as Secchi transparency. The dissolved oxygen electrode method uses a selective membrane to allow the dissolved oxygen in the water to pass through to isolate it from liquids, ions and other interfering substances. The molecular oxygen passing through the membrane is then reduced at the electrode cathode. The current intensity generated in a steady state is proportional to the dissolved oxygen concentration; thus, the current value can be converted to the dissolved oxygen concentration in the water. Table 1 presents the detailed geo-temporal information and testing results with respect to six sample-collecting sites in the pond. The sampling process of three experimental sets was completed on different dates and times, respectively. As the pond is small and we assume that water quality parameters are considered stably constant during a short period, the sampling date/time for S1~S6 in each sampling process, thus, can be assumed the same as well.

Table 1. The corresponding coordinate positions of sampling points and the results of the water quality parameters analyzed by SGS Taiwan. Among them S1, S1′, S1″ refer to sampling at the same place but at different time intervals.

Sampling Point	Coordinate Position	Sampling Date/Time	Chlorophyll a (μg/L)	Total Phosphorus (μg/L)	Transparency (m)	Dissolved Oxygen (mg/L)
S1	24°08′38″ N 120°41′02″ E	5/15 AM 10:00	69.8	94	0.47	16.7
S2	24°08′39″ N 120°41′03″ E	5/15 AM 10:00	67.3	65	0.50	21.1
S3	24°08′38″ N 120°41′05″ E	5/15 AM 10:00	51.4	65	0.57	21.7
S4	24°08′35″ N 120°41′04″ E	5/15 AM 10:00	58.5	78	0.60	21.0

Table 1. *Cont.*

Sampling Point	Coordinate Position	Sampling Date/Time	Chlorophyll a (μg/L)	Total Phosphorus (μg/L)	Transparency (m)	Dissolved Oxygen (mg/L)
S5	24°08′34″ N 120°41′04″ E	5/15 AM 10:00	61.9	65	0.61	20.6
S6	24°08′35″ N 120°41′01″ E	5/15 AM 10:00	55.4	65	0.58	18.8
S1′	24°08′38″ N 120°41′02″ E	6/14 AM 11:00	116	94	0.40	9.0
S2′	24°08′39″ N 120°41′03″ E	6/14 AM 11:00	103	97	0.47	9.6
S3′	24°08′38″ N 120°41′05″ E	6/14 AM 11:00	91.8	126	0.41	9.2
S4′	24°08′35″ N 120°41′04″ E	6/14 AM 11:00	88.1	113	0.36	8.8
S5′	24°08′34″ N 120°41′04″ E	6/14 AM 11:00	73.2	104	0.42	9.2
S6′	24°08′35″ N 120°41′01″ E	6/14 AM 11:00	107	96	0.45	9.7
S1″	24°08′38″ N 120°41′02″ E	6/19 AM 10:30	56	65	0.60	19.4
S2″	24°08′39″ N 120°41′03″ E	6/19 AM 10:30	50.1	58	0.56	19.2
S3″	24°08′38″ N 120°41′05″ E	6/19 AM 10:30	64.7	65	0.71	17.0
S4″	24°08′35″ N 120°41′04″ E	6/19 AM 10:30	70.2	53	0.68	16.2
S5″	24°08′34″ N 120°41′04″ E	6/19 AM 10:30	49.7	58	0.55	17.2
S6″	24°08′35″ N 120°41′01″ E	6/19 AM 10:30	53.5	63	0.48	16.0

3.2. UAV Multispectral Surveys

As shown in Figure 2, an octocopter (Tarot X8) with a pan-tilt system and a commercial multispectrometer (Micasence Altum) were utilized for data collection. The flight time was during 10:00 am–11:00 am, which was established with regard to the sunlight angle to minimize the sun-glint effects and the specular reflections. Six ground control points were evenly distributed in the flight area. The x, y and z coordinates were surveyed with a GPS with sub-metric precision. The camera had five multispectral bands, i.e., red (668 nm center, 14 nm bandwidth), green (560 nm center, 27 nm bandwidth), blue (475 nm center, 32 nm bandwidth), red edge (717 nm center, 12 nm bandwidth) and near infrared (NIR) (842 nm center, 57 nm bandwidth) and one thermal image sensor (Longwave infrared 8–14 μm). The fields of view of the multispectral and thermal sensors were 48° × 37° and 57° × 44°, respectively. The multispectral and thermal images from this camera can be acquired at 1 s intervals. In addition, the system had a calibrated reflective panel and a sunlight sensor, which can measure the instantaneous energy from the sun. The GPS system built into the irradiance sensor can be used to save geotagged images. The multispectrometer Micasence Altum mainly utilized the 'global shutter' technique to acquire all image pixels at a time rather than the 'rolling shutter' technique to line scan image pixels, which leads to no time interval for the same frame of image. The maximal sample point the camera can detect is 2064 × 1544 pixels for five multispectral bands except the thermal image band. When

the UAV flight mission was planned at 15 m height, the spatial resolution of the captured spectral image was approximately 1 cm and the detected ground area of a captured image was estimated as 20.6 × 15.4 m^2. Certainly, the detected area may vary depending on the flight altitude.

Figure 2. Octocopter (Tarot X8) with a pan-tilt system and a commercial multispectrometer (Micasence Altum).

Practical experience has shown that the quality of collected multispectral images is greatly dependent on the atmospheric conditions and geometric factors. Regarding the atmospheric conditions, the reflected light in terms of electromagnetic energy can be influenced by the angle of reflection, particles in the air and cloud shadow, etc., while geometric factors primarily concern the characteristics of specular, near-specular, near-diffuse or diffuse reflection. Strong mirror-like reflections on the surface of water should be avoided while UAV-based multispectral images are recorded. Further, stable control of the UAV flight is considered necessary and critical to improve the image quality. To eliminate these potential measurement errors, several essential procedures to calibrate the multispectral image are essentially required. Before the application of UAV imagery to multiple regression models, a series of image pre-processing steps needs to be completed. First, the raw image data, referred to as digit number (DN), are in the form of 16-bit and ranging from 0 to approximately 65,535 values, which cannot be directly employed to calculate corresponding reflectance. Instead, a calibrated reflectance panel (CRP) with accurate reflectance between 400 nm and 850 nm wavelength is introduced to adjust DN values to carry out the relative radiometric calibration. Via relative radiometric calibration, the reflectance of a specific spatial pixel is, therefore, defined as follows:

$$\text{Reflectance}_{(x,y)} = \frac{\text{DN}_{(x,y)}}{\text{DN}_{\text{panel}}} \quad (1)$$

$\text{Reflectance}_{(x,y)}$: the reflectance of a pixel (x,y) from the spectral image;
$\text{DN}_{(x,y)}$: DN value of a pixel (x,y) from the spectral image;
DN_{panel}: DN value of the CRP from the spectral image.

Further, the multispectral image camera provides a GPS and a downwelling light sensor (DLS) to precisely record temporal and spatial positions, as well as the ambient intensity and the incident angle of sunlight for each multispectral band, which can be embedded into the image file format (.tiff) for supplementary calibration of reflectance. In addition, the calibration of optical vignetting is also taken into account to adjust the reduced light intensity (i.e., DN value) of image pixels around the corner areas in a picture. The vignetting phenomenon is mainly due to the set up and distance variation between camera lens and the photo-sensitive device, but it can be easily calibrated by lots of commercial software at present. Using these calibration processes introduced above, a schematic example of the multispectral image before/after calibration processing is shown in Figure 3, and one can tell the slight adjustment at the corresponding pixel in each image.

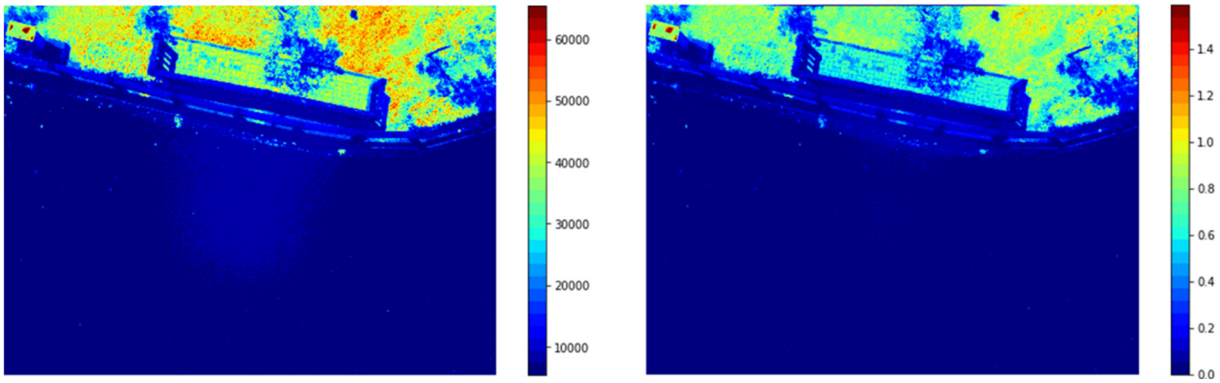

Figure 3. The UAV-based multispectral image from Micasence Altum before calibration (**left**, color bar unit: DN) and after calibration (**right**, color bar unit: reflectance).

3.3. Multispectral Regression Modeling for Water Quality

In this study, we inspected four water quality parameters, including chlorophyll a, total phosphorus, transparency and dissolved oxygen. For the individual water quality parameter, the possible interpretation of regression models could be in the forms of linear, band ratio and even logarithmic expression. More essentially, the contribution of multispectral bands into the individual water quality parameter should be taken into account. These resulted in thorough consideration through a total 76 combinations of regression models, i.e., $y = f(N_i)$, as explained in more detail as follows:

(1) *Single-band linear regression*: $y = a \times N + b$, where a and b are the regression coefficients, totally five models.
(2) *Band-ratio regression:* $y = a \times (N_1/N_2) + b$, where a and b are the regression coefficients, totally 20 models.
(3) *Single-band logarithmic regression*: $Ln(y) = a \times Ln(N) + b$, where a and b are the regression coefficients, totally five models.
(4) *Band-ratio logarithmic regression*: $Ln(y) = a \times Ln(N_1/N_2) + b$, where a and b are the regression coefficients, totally 20 models.
(5) *Multi-band linear regression:* $y = a \times N_1 + b \times N_2 + c \times N_3 + d \times N_4 + e \times N_5$, where a, b, c, d and e are the regression coefficients, totally 26 models.

4. Results and Discussion

The proposed statistical modeling approach using UAV-based multispectral imagery aims to perform a rapid and cost-effective valuation of the water eutrophication state by calculating CTSI values quantitatively. So far, the on-site sampling inspection via biochemical analysis in a laboratory has been widely adopted to quantify and validate the pollutant concentrations in official assessments. However, the expensive and time-consuming process is still a significant disadvantage to deal with more urgent and challenging requests from environmental protection and conservation worldwide. The presented method is expected to carry out scientifically sound modeling evaluations with a limited number of biochemical inspection samples, and to provide accurate and timely forecast of the water quality parameters at any position of interest without extensive biochemical inspection tests.

We use both multispectrometer and on-site water quality sampling analysis to obtain three sets of water quality parameters on different dates by selecting six different sampling points. Therefore, there are 18 data points available for calculation in statistical and chemical analysis, respectively. However, to verify the accuracy of these regression models, we employ only 12 of these data points at random for regression analysis and the other 6 data points are kept for validation of relevant results obtained from regression models and on-site tests.

After the analysis and comparison of the results of a total of 76 regression models, each water quality parameter is able to find the optimal model, which is defined by

possessing the largest coefficient of determination (R^2) that measures how well a statistical model predicts an outcome, i.e., $0 \leq R^2 \leq 1$. To conclude the comparison, the band-ratio logarithmic regression model for chlorophyll a, the single-band logarithmic regression model for total phosphorus, the single-band regression model for transparency and the band-ratio logarithmic regression model for dissolved oxygen with specific spectral bands show the largest coefficients of determination, respectively. Table 2 presents the optimal regression equations of the chlorophyll a, total phosphorus, transparency and dissolved oxygen with the reflectance factors of red, red edge and green bands, which are assumed to play the key roles of feature bands in association with the correlated parameters.

Table 2. The optimal regression results of chlorophyll a, concentration of total phosphorus, transparency and dissolved oxygen in this study, where N_{RE} is reflectance of red edge band (717 nm), N_R is reflectance of red band (668 nm) and N_G is reflectance of green band (560 nm).

Water Quality Parameter, (y)	Coefficient of Determination (R^2)	Optimal Multispectral Regression Model
Chlorophyll a	0.8154	$\mathrm{Ln(y)} = 5.8696 \times \mathrm{Ln}\left(\frac{N_{RE}}{N_R}\right) + 2.3998$
Total phosphorus	0.8086	$\mathrm{Ln(y)} = -2.7448 \times \mathrm{Ln}(N_R) - 1.3247$
Transparency	0.9406	$\mathrm{(y)} = 8.5635 \times (N_R) - 0.5747$
Dissolved oxygen	0.7339	$\mathrm{Ln(y)} = -2.3986 \times \mathrm{Ln}\left(\frac{N_G}{N_R}\right) + 3.3716$

As shown in Figure 4, the best coefficients of determination (R^2) of the regression models for chlorophyll a, total phosphorus concentration, transparency and dissolved oxygen were found to be 0.8154, 0.8086, 0.9406 and 0.7339, respectively, which are acceptable for regression analysis and mathematical modeling. The corresponding values of root mean square error (RMSE) for these regression models were 8.5373, 7.9580, 0.0194 and 2.6343, respectively. Among them, particularly, the very small RMSE value in the transparency model reflected excellent precision in data concentration along the line of best fit.

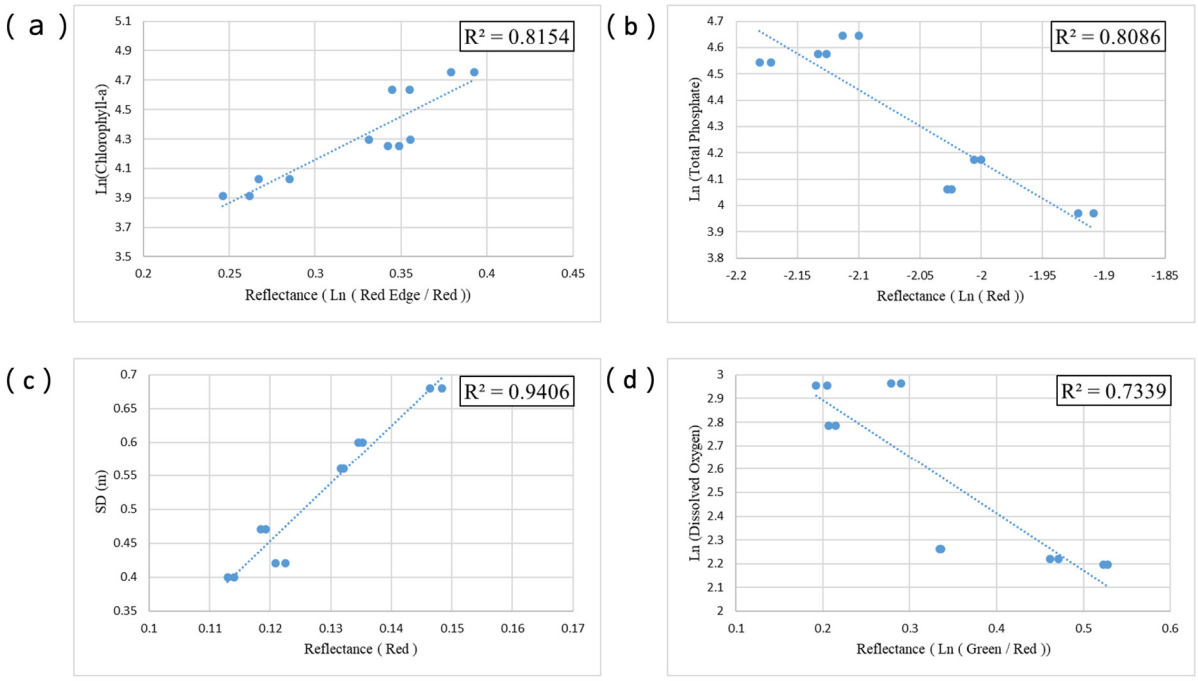

Figure 4. The coefficients of determination of the regression models: (**a**) chlorophyll a, (**b**) total phosphorus concentration, (**c**) transparency and (**d**) dissolved oxygen.

Regarding the definition of Carlson trophic state index, it is employed to represent the trophic state of the lake water at a specific sampling position. If the CTSI value calculated is less than 40, it is called oiligotrophic; if 40~50, mesotrophic; if 50~70, eutrophic; and if CTSI is greater than 70, it is called hypereutrophic [36,37]. The CTSI value was mainly calculated using the following Formula (2), which is a judgment standard that uses multiple parameters to summarize:

$$\mathrm{CTSI} = \frac{[\mathrm{TSI(SD)} + \mathrm{TSI(CHL)} + \mathrm{TSI(TP)}]}{3} \quad (2)$$

where SD is the transparency of water measured with the Secchi disk (m), TP is the concentration of total phosphorus in water ($\mu g \cdot L^{-1}$) and CHL is the concentration of chlorophyll a in water ($\mu g \cdot L^{-1}$). The Trophic State Indices (TSI) for three environmental parameters were calculated by the following Formulas (3)–(5), respectively [36].

$$\mathrm{TSI(SD)} = 60 - 14.41 \times \ln(\mathrm{SD}) \quad (3)$$

$$\mathrm{TSI(CHL)} = 9.81 \times \ln(\mathrm{CHL}) + 30.6 \quad (4)$$

$$\mathrm{TSI(TP)} = 14.42 \times \ln(\mathrm{TP}) + 4.15 \quad (5)$$

After completing the verification of the water quality parameter regression models, the reflectance after the multispectral image conversion was substituted into the regression equations of the best water quality parameter models to estimate or forecast chlorophyll a, total phosphorus, water transparency and dissolved oxygen at 12 sampling positions in the pond, as shown in Figure 5. The equations for calculating the forecast CTSI value were incorporated and then compared with the real CTSI value calculated through the biochemical analysis results. As shown in Table 3, it was found that the resultant CTSI model demonstrated relatively satisfactory forecast capability, in which the largest CTSI error between the real and predicted CTSI values was 1.4% only at validation point 6, and the RMSE value for all six validation results was as small as 0.6624, strongly indicating that the proposed water quality regression models are favorably feasible for expressing the degree of water eutrophication in terms of CTSI forecast modeling. The CTSI values of six sampling points calculated by either SGS analysis or multispectral regression modeling both revealed a high eutrophic to hypereutrophic state of Sun Moon Pond due to regular human leisure activities and excessive excrement of city animals residing around the pond.

Table 3. Comparison of Carlson trophic state index (CTSI) values calculated by the regression models and SGS analysis data. Validation points 1~6 were randomly selected from Table 1 for model validation.

Validation Point	CTSI Calculated by the Regression Model	CTSI Calculated from the SGS Data	CTSI Error (%)
1	74.17	73.37	1.1
2	71.92	72.35	0.6
3	72.09	72.11	0.02
4	67.34	67.26	0.1
5	67.17	66.68	0.7
6	65.46	66.42	1.4

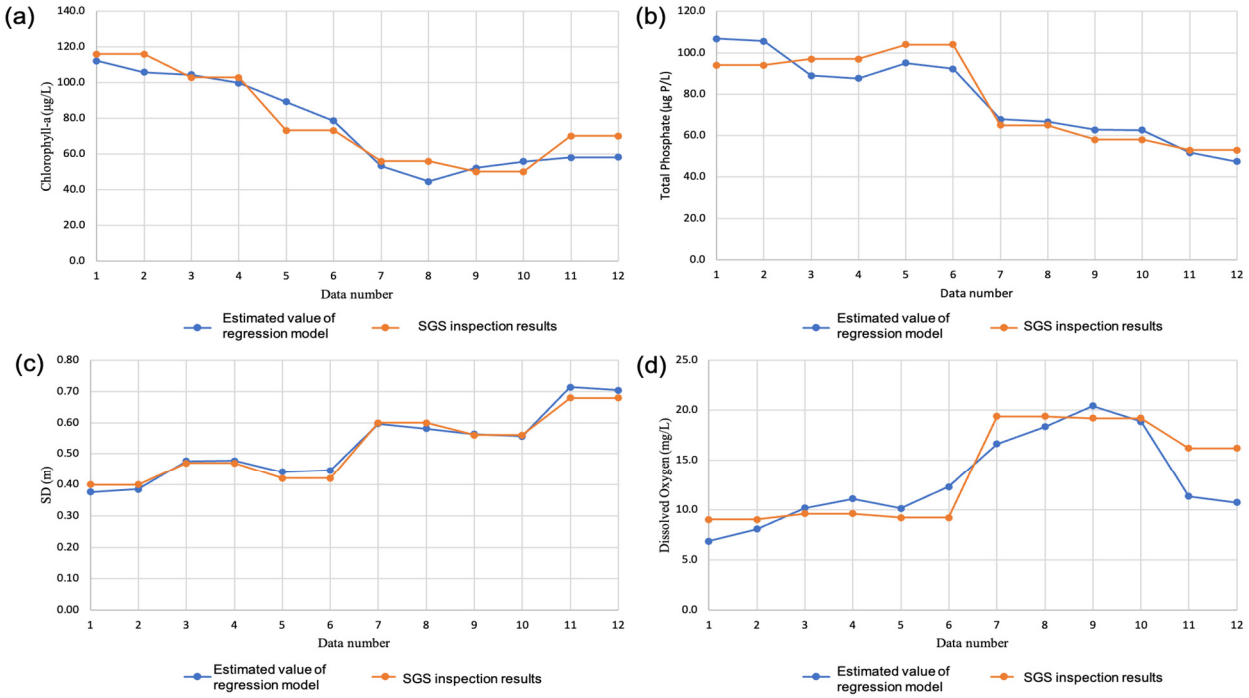

Figure 5. Comparison of water quality parameters obtained from multispectral interpretation models and SGS inspection results: (**a**) chlorophyll a, (**b**) total phosphorus concentration, (**c**) transparency, (**d**) dissolved oxygen.

As previously mentioned, this study aims to explore the CTSI value using the reflectance obtained by the drone equipped with a multispectrometer, and one can use this trophic index to assess the comprehensive trophic state of the water in an ecosystem. The experimental results showing small CTSI errors with a small RMSE imply that we can apply multispectral raw data aligned with limited biochemical tests to estimate the CTSI value without massive sampling requirements. However, the current work in this study is merely applied to a small pond or lake that is not directly related to a river or a natural water source whose monitoring condition is much more complicated. Further, more advanced requirements of detection facility that can produce high throughput of image data over a larger lake area will definitely increase in this application field. It is evident that more advances in both UAV and multispectral sensor (cameras) specifications, and intelligent algorithmic development for appropriate regression modeling, may continue to utilize the proposed methodology.

To date, the proposed regression modeling approach is proven to work, so we are interested in extending these models more widely to find the appropriate and real-time expressions for more water quality parameters combined with emerging artificial intelligence (AI) feature recognition and big data analysis techniques in the near future. In addition, the visualization maps of individual water quality parameters, such as concentration distribution, temporal variation, etc., using the proposed method are currently in progress in our lab and these results will be disclosed soon in the subsequent manuscript.

5. Conclusions

For the first time, this short article proposes a real-time and low-cost approach to assess the Carlson trophic state index (CTSI) of a water ecosystem. Through the multispectral image provided by a low-altitude UAV, we can establish the corresponding regression models of different biochemical substances with respect to the multispectral reflectance in different optical spectral bands and statistically align with the data of the biochemical sampling tests. These regression models are then employed to estimate the water quality parameters, including chlorophyll a, total phosphorus and transparency, to generate the

Carlson Indices of interest. It is found that the maximal error in CTSI accuracy was only 1.4% and the root mean square error was 0.6624. With the successful forecast of CTSI values by analyzing the multispectral images, we believe that the cost-effective method can exhibit a rapid and reliable solution for observing the quantitative change in water quality features.

Author Contributions: C.-Y.L. and C.-C.L. were responsible for coordinating, writing and revising the article. C.-Y.L., J.T.H.T. and C.-C.L. decided the methodology and data analysis with constructive discussions. M.-S.T. and C.-Y.L. prepared the materials and equipment and performed these UAV experiments. All authors have read and agreed to the published version of the manuscript.

Funding: This research was co-funded by the Ministry of Science and Technology, Taiwan, and Rdata system Co., Ltd., Taiwan under the grants No. MOST 109-2622-E-027-012-CC3 and MOST 111-2622-E-027-010.

Institutional Review Board Statement: Not applicable.

Informed Consent Statement: Not applicable.

Data Availability Statement: Not applicable.

Conflicts of Interest: The authors declare no conflict of interest.

References

1. Sun, J.; Wang, J.; Wang, T.; Zhang, T. Urbanization, economic growth, and environmental pollution: Partial differential analysis based on the spatial Durbin model. *Manag. Environ. Qual.* **2019**, *30*, 483–494. [CrossRef]
2. Zhang, K.; Shen, J.; He, R.; Fan, B.; Han, H. Dynamic Analysis of the Coupling Coordination Relationship between Urbanization and Water Resource Security and Its Obstacle Factor. *Int. J. Environ. Res. Public Health* **2019**, *16*, 4765. [CrossRef] [PubMed]
3. Zhang, Y.; Sun, M.; Yang, R.; Li, X.; Zhang, L.; Li, M. Decoupling water environment pressures from economic growth in the Yangtze River Economic Belt, China. *Ecol. Indic.* **2021**, *122*, 107314. [CrossRef]
4. Patnaik, R. Impact of Industrialization on Environment and Sustainable Solutions—Reflections from a South Indian Region. *IOP Conf. Ser. Earth Environ. Sci.* **2018**, *120*, 012016. [CrossRef]
5. Liu, Y.; Yang, L.; Jiang, W. Coupling coordination and spatiotemporal dynamic evolution between social economy and water environmental quality—A case study from Nansi Lake catchment, China. *Ecol. Indic.* **2020**, *119*, 106870. [CrossRef]
6. Liou, S.-M.; Lo, S.-L.; Wang, S.-H. A Generalized Water Quality Index for Taiwan. *Environ. Monit. Assess.* **2004**, *96*, 35–52. [CrossRef]
7. Lin, C.; Chen, C.; Kao, C.; Hong, A.; Wu, C. Development of the sediment and water quality management strategies for the Salt-water River, Taiwan. *Mar. Pollut. Bull.* **2011**, *63*, 528–534. [CrossRef]
8. Chow, M.F.; Shiah, F.K.; Lai, C.C.; Kuo, H.Y.; Wang, K.W.; Lin, C.H.; Chen, T.Y.; Kobayashi, Y.; Ko, C.Y. Evaluation of surface water quality using multivariate statistical techniques: A case study of Fei-Tsui Reservoir basin, Taiwan. *Environ. Earth Sci.* **2015**, *75*, 6. [CrossRef]
9. Putri, M.S.A.; Lou, C.-H.; Syai'In, M.; Ou, S.-H.; Wang, Y.-C. Long-Term River Water Quality Trends and Pollution Source Apportionment in Taiwan. *Water* **2018**, *10*, 1394. [CrossRef]
10. López-García, M.J.; Caselles, V. Use of Thematic Mapper data to assess water quality in Albufera lagoon of Valencia (Spain). In Proceedings of the 13th Annual Conference of the Remote Sensing Society, Nottingham, UK, 7–11 September 1987; pp. 510–519.
11. Dona, C.; Sanchez, J.M.; Caselles, V.; Dominguez, J.A.; Camacho, A. Empirical relationships for monitoring water quality of lakes and reservoirs through multispectral images. *IEEE J. Sel. Top. Appl. Earth Obs. Remote Sens.* **2014**, *7*, 1632–1641. [CrossRef]
12. Dekker, A.; Malthus, T.; Seyhan, E. Quantitative modeling of inland water quality for high-resolution MSS systems. *IEEE Trans. Geosci. Remote. Sens.* **1991**, *29*, 89–95. [CrossRef]
13. Cillero Castro, C.; Domínguez Gómez, J.A.; Delgado Martín, J.; Hinojo Sánchez, B.A.; Cereijo Arango, J.L.; Cheda Tuya, F.A.; Díaz-Varela, R. An UAV and Satellite Multispectral Data Approach to Monitor Water Quality in Small Reservoirs. *Remote Sens.* **2020**, *12*, 1514. [CrossRef]
14. Pu, H.; Liu, D.; Qu, J.-H.; Sun, D.-W. Applications of Imaging Spectrometry in Inland Water Quality Monitoring—A Review of Recent Developments. *Water Air Soil Pollut.* **2017**, *228*, 131. [CrossRef]
15. Kwon, Y.S.; Jang, E.; Im, J.; Baek, S.H.; Park, Y.; Cho, K.H. Developing data-driven models for quantifying Cochlodinium polykrikoides using the Geostationary Ocean Color Imager (GOCI). *Int. J. Remote Sens.* **2017**, *39*, 68–83. [CrossRef]
16. Zhang, W.; Liu, Z. Daily water quality evaluation of reservoir and cyanobacteria pollution index calculation. *Water Supply* **2020**, *21*, 836–847. [CrossRef]
17. Liu, J.; Zhang, Y.; Yuan, D.; Song, X. Empirical Estimation of Total Nitrogen and Total Phosphorus Concentration of Urban Water Bodies in China Using High Resolution IKONOS Multispectral Imagery. *Water* **2015**, *7*, 6551–6573. [CrossRef]
18. El Din, E.S.; Zhang, Y. Estimation of both optical and nonoptical surface water quality parameters using Landsat 8 OLI imagery and statistical techniques. *J. Appl. Remote Sens.* **2017**, *11*, 046008. [CrossRef]

19. Du, C.; Wang, Q.; Li, Y.; Lyu, H.; Zhu, L.; Zheng, Z.; Wen, S.; Liu, G.; Guo, Y. Estimation of total phosphorus concentration using a water classification method in inland water. *Int. J. Appl. Earth Obs. Geoinf.* **2018**, *71*, 29–42. [CrossRef]
20. McEliece, R.; Hinz, S.; Guarini, J.-M.; Coston-Guarini, J. Evaluation of Nearshore and Offshore Water Quality Assessment Using UAV Multispectral Imagery. *Remote Sens.* **2020**, *12*, 2258. [CrossRef]
21. Erena, M.; Domínguez, J.A.; Aguado-Giménez, F.; Soria, J.; García-Galiano, S. Monitoring Coastal Lagoon Water Quality through Remote Sensing: The Mar Menor as a Case Study. *Water* **2019**, *11*, 1468. [CrossRef]
22. Wang, F.; Hu, H.; Luo, Y.; Lei, X.; Wu, D.; Jiang, J. Monitoring of Urban Black-Odor Water Using UAV Multispectral Data Based on Extreme Gradient Boosting. *Water* **2022**, *14*, 3354. [CrossRef]
23. Cui, M.; Sun, Y.; Huang, C.; Li, M. Water Turbidity Retrieval Based on UAV Hyperspectral Remote Sensing. *Water* **2022**, *14*, 128. [CrossRef]
24. Xiao, Y.; Guo, Y.; Yin, G.; Zhang, X.; Shi, Y.; Hao, F.; Fu, Y. UAV Multispectral Image-Based Urban River Water Quality Monitoring Using Stacked Ensemble Machine Learning Algorithms—A Case Study of the Zhanghe River, China. *Remote Sens.* **2022**, *14*, 3272. [CrossRef]
25. Masoud, A.A. On the Retrieval of the Water Quality Parameters from Sentinel-3/2 and Landsat-8 OLI in the Nile Delta's Coastal and Inland Waters. *Water* **2022**, *14*, 593. [CrossRef]
26. Lee, C.-H.; Liu, L.-W.; Wang, Y.-M.; Leu, J.-M.; Chen, C.-L. Drone-Based Bathymetry Modeling for Mountainous Shallow Rivers in Taiwan Using Machine Learning. *Remote Sens.* **2022**, *14*, 3343. [CrossRef]
27. Kezoudi, M.; Keleshis, C.; Antoniou, P.; Biskos, G.; Bronz, M.; Constantinides, C.; Desservettaz, M.; Gao, R.-S.; Girdwood, J.; Harnetiaux, J.; et al. The Unmanned Systems Research Laboratory (USRL): A New Facility for UAV-Based Atmospheric Observations. *Atmosphere* **2021**, *12*, 1042. [CrossRef]
28. Änäkkälä, M.; Lajunen, A.; Hakojärvi, M.; Alakukku, L. Evaluation of the Influence of Field Conditions on Aerial Multispectral Images and Vegetation Indices. *Remote Sens.* **2022**, *14*, 4792. [CrossRef]
29. Kim, J.; Kim, S.; Ju, C.; Son, H.I. Unmanned Aerial Vehicles in Agriculture: A Review of Perspective of Platform, Control, and Applications. *IEEE Access* **2019**, *7*, 105100–105115. [CrossRef]
30. Mazzia, V.; Comba, L.; Khaliq, A.; Chiaberge, M.; Gay, P. UAV and Machine Learning Based Refinement of a Satellite-Driven Vegetation Index for Precision Agriculture. *Sensors* **2020**, *20*, 2530. [CrossRef]
31. Cao, Y.; Li, G.L.; Luo, Y.K.; Pan, Q.; Zhang, S.Y. Monitoring of sugar beet growth indicators using wide-dynamic-range veg-etation index (WDRVI) derived from UAV multispectral images. *Comput. Electron. Agric.* **2020**, *171*, 105331. [CrossRef]
32. Zheng, C.; Abd-Elrahman, A.; Whitaker, V.; Dalid, C. Prediction of Strawberry Dry Biomass from UAV Multispectral Imagery Using Multiple Machine Learning Methods. *Remote Sens.* **2022**, *14*, 4511. [CrossRef]
33. Ahmad, A.; Gilani, H.; Ahmad, S. Forest Aboveground Biomass Estimation and Mapping through High-Resolution Optical Satellite Imagery—A Literature Review. *Forests* **2021**, *12*, 914. [CrossRef]
34. Johansen, K.; Morton, M.J.L.; Malbeteau, Y.; Aragon, B.; Al-Mashharawi, S.; Ziliani, M.; Angel, Y.; Fiene, G.; Negrao, S.; Mousa, M.A.A.; et al. Predicting Biomass and Yield at Harvest of Salt-Stressed Tomato Plants Using Uav Imagery. *Int. Arch. Photogramm. Remote Sens. Spat. Inf. Sci.* **2019**, *XLII-2/W13*, 407–411. [CrossRef]
35. Environmental Protection Agency, Executive Yuan, Taiwan, ROC, Water Quality Category. Available online: https://www.epa.gov.tw/niea/32A85B63C9EC18C0 (accessed on 12 December 2022).
36. Carlson, R.E. A trophic state index for lakes. *Limnol. Oceanogr.* **1977**, *22*, 361–369. [CrossRef]
37. Kratzer, C.R.; Brezonik, P.L. A Carlson-Type Trophic State Index for Nitrogen in Florida Lakes. *J. Am. Water Resour. Assoc.* **1981**, *17*, 713–715. [CrossRef]